Published online 31 August 2023 *Nucleic Acids Research, 2023, Vol. 51, No. 18* **9629–9642**
https://doi.org/10.1093/nar/gkad681

DNA mimic foldamers affect chromatin composition and disturb cell cycle progression

Vera Kleene[1], Valentina Corvaglia[2], Erika Chacin[1], Ignasi Forne[3], David B. Konrad[2], Pardis Khosravani[4], Céline Douat[2], Christoph F. Kurat[1], Ivan Huc[2] and Axel Imhof[1,3,*]

[1]Department of Molecular Biology, Biomedical Center Munich, Faculty of Medicine, Ludwig-Maximilians University, Großhaderner Strasse 9, 82152 Planegg-Martinsried, Germany, [2]Department of Pharmacy, Institute of Chemical Epigenetics, Ludwig-Maximilians University, Butenandtstraße 5-13, 81377 München, Germany, [3]Protein Analysis Unit, Biomedical Center Munich, Faculty of Medicine, Ludwig-Maximilians University, Großhaderner Strasse 9, 82152 Planegg-Martinsried, Germany and [4]Core Facility Flow Cytometry, Biomedical Center, Faculty of Medicine, Ludwig-Maximilians-University Munich, 82152 Planegg-Martinsried, Germany.

Received February 16, 2023; Revised August 02, 2023; Editorial Decision August 03, 2023; Accepted August 10, 2023

ABSTRACT

The use of synthetic chemicals to selectively interfere with chromatin and the chromatin-bound proteome represents a great opportunity for pharmacological intervention. Recently, synthetic foldamers that mimic the charge surface of double-stranded DNA have been shown to interfere with selected protein–DNA interactions. However, to better understand their pharmacological potential and to improve their specificity and selectivity, the effect of these molecules on complex chromatin needs to be investigated. We therefore systematically studied the influence of the DNA mimic foldamers on the chromatin-bound proteome using an *in vitro* chromatin assembly extract. Our studies show that the foldamer efficiently interferes with the chromatin-association of the origin recognition complex *in vitro* and *in vivo*, which leads to a disturbance of cell cycle in cells treated with foldamers. This effect is mediated by a strong direct interaction between the foldamers and the origin recognition complex and results in a failure of the complex to organise chromatin around replication origins. Foldamers that mimic double-stranded nucleic acids thus emerge as a powerful tool with designable features to alter chromatin assembly and selectively interfere with biological mechanisms.

GRAPHICAL ABSTRACT

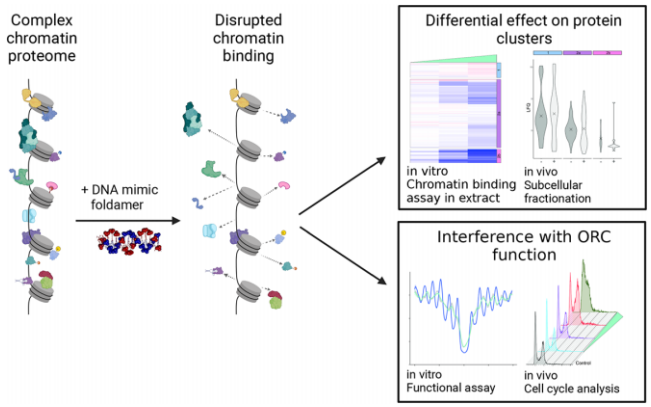

INTRODUCTION

In the eukaryotic nucleus, DNA is associated with many proteins to form a highly dynamic chromatin structure that modulates gene expression, allows the cell to ensure the efficient repair of damaged DNA, and guarantees a faithful replication of DNA during cell division (1–3). Over the last years, several general approaches have been pursued to characterize the chromatin-bound proteome in higher eukaryotes (4–7). These studies underscored the enormous complexity of chromatin, which goes way beyond the mere assembly of histones and DNA. Moreover, chromatin capture technologies revealed a highly dynamic network of interactions in the nucleus mediated by the chromatin-bound proteome (4,8–11). The molecular principles and interactions that drive these structures are still not fully understood and range from strong and specific protein–DNA or protein–protein interactions (1) to weak and more generic

*To whom correspondence should be addressed. Tel: +49 89 218075420; Fax: +49 89 218075410; Email: imhof@lmu.de
Present address: Valentina Corvaglia, Institute for Stem-Cell Biology, Regenerative Medicine and Innovative Therapies, IRCCS Casa Sollievo della Sofferenza, San Giovanni Rotondo, Italy & Center for Nanomedicine and Tissue Engineering (CNTE), ASST Grande Ospedale Metropolitano Niguarda, Milan, Italy.

interactions involving the overall shape of B-DNA rather than defined sequences (12,13). During every cell division, DNA is duplicated, and novel chromatin is assembled in a very complex and highly coordinated process that ensures the stable maintenance of its structure (14). A similar reliable chromatin re-assembly also operates during DNA repair (10,15,16). Thanks to this complex system involving multiple players, the chromatin structure is faithfully copied during replication and upon the resolution of DNA damage. These reliable assemblies of specific chromatin structures occur in the presence of multiple proteins that have various affinities to chromatin and engage in protein-nucleic acid interactions as well as protein–protein interactions. The selective interference with only certain types of interactions could help decipher individual roles within the complex and dynamic network of interactions at play. However, tools able of such selective interference have been lacking. Here, we present the investigation of an *in vitro* chromatin assembly system from *Drosophila* embryos in presence of a synthetic foldamer mimicking the overall shape and negative charge distribution of double-stranded DNA.

We have previously reported the design and structure elucidation of oligoamides in which monomers $^{m}Q^{Pho}$ and Q^{Pho} alternate (Figure 1A structure **1**) adopting a B-DNA like shape and charge distribution (17,18). Because of these properties, the DNA mimic foldamers have been proposed as candidates to bind to and interfere with the functions of non-sequence selective DNA-binding proteins. In the past we have shown that the foldamers interfere with the DNA binding of purified Top1 and HIV-IN, resulting in a strong inhibition of these proteins *in vitro* (17,18). In their mode of action, the DNA mimic foldamers are reminiscent of DNA mimic proteins (19,20), naturally occurring proteins that also mimic the shape and charge distribution of nucleic acids and highjack DNA-binding proteins. Their oligoamide nature and their ability to compete with DNA-protein interactions make them conceptually (though not structurally) related to other oligoamides (21–23) that do not mimic DNA but instead bind to DNA and may be used as specific tools to modulate gene expression *in vivo* (24–26). Neither class of compounds has been exploited in a systematic approach to study chromatin binding in a complex mixture or in cells.

Our study shows that the DNA mimic foldamers interfere with several known chromatin factors with variable efficiency. One of the most striking effects was the binding to, and competition for the interaction with DNA by the origin recognition complex (ORC). In higher eukaryotes, the hexameric ORC complex marks the origin of replication throughout the cell cycle and mediates the loading of the DNA helicase complex MCM1–7 upon activation in the G1 phase. Besides this major role in DNA replication, the ORC complex has also been shown to play a role in RNA export (27) and in setting up a defined chromatin structure around the replication origins (28). While ORC binds to a defined DNA sequence in yeast, replication origins in higher eukaryotes do not have a well-defined DNA sequence to which ORC binds. Nevertheless, replication originates at specific sites, which have been suggested to be defined by a combination of factors including DNA topology, local chromatin structure, and local histone modifications (29–32). The ability to interfere with the chromatin binding of ORC or similar factors by using synthetic molecules, therefore, provides novel ways to better understand the principles of their interactions with chromatin and to interfere with their function.

MATERIALS AND METHODS

Reagents and analytical methods for foldamer synthesis

Chemical reagents were purchased from commercial suppliers (Abcr, Fisher Scientific, Merck, Sigma-Aldrich, TCI, or VWR) and used without further purification. Low loading (LL) Wang resin (100–200 mesh, 1% DVB, manufacturer's loading: 0.41 mmol g^{-1}) was purchased from Novabiochem. Peptide grade *N*,*N*-dimethylformamide (DMF) was purchased from Carlo Erba. Anhydrous chloroform and trimethylamine (TEA) were obtained via distillation over CaH_2 prior to use. Anhydrous tetrahydrofuran (THF) was obtained via an MBRAUN SPS800 solvent purification system. Ultrapure water was obtained via a Sartorius arium® pro VF ultrapure water system and used with RP-HPLC quality acetonitrile for RP-HPLC analyses and purifications. Analytical and semi-preparative RP-HPLC were performed on a Thermo Fisher Scientific Ultimate 3000 HPLC System using Macherey-Nagel Nucleodur C18 HTec columns (4 × 100 mm, 5 μm and 10 × 250 mm, 5 μm) and Macherey-Nagel Nucleodur C8 Gravity columns (4 × 50 mm, 5 μm and 10 × 100 mm, 5 μm) at 1 ml/min (4 mm columns) or 5 ml/min (10 mm columns). UV absorbance was monitored at 300 nm. For the protected precursor of foldamer **1**, prior to the semi-preparative RP-HPLC, an additional purification step was performed using a Waters LC Prep 150 System equipped with a quaternary gradient module at 25 ml/min. The mobile phase was composed of 12.5 mM triethylammonium acetate (TEAA) in water pH 8.5 (solvent A) and 12.5 mM TEAA in water: acetonitrile 1:2 vol/vol pH 8.5 (solvent B) for foldamers **1** and **2**. For the protected precursor of foldamer **1**, it was composed of water +0.1% TFA (solvent A) and acetonitrile + 0.1% TFA (solvent B). Nuclear magnetic resonance (NMR) spectra were recorded on an Avance III HD 500 MHz Bruker BioSpin spectrometer equipped with broadband observe 5-mm BB-H&FD CryProbeTM Prodigy. Measurements were performed at 25°C. Water suppression was performed with excitation sculpting. Processing was done with MestReNova (v.12.0.0–20080) NMR processing software from Mestrelab Research. Chemical shifts are reported in ppm. High-resolution liquid chromatography–mass spectrometry (HR LC-MS) analyses were recorded on a Bruker microTOF II (in either positive or negative ionization mode) equipped with a Thermo Fisher Scientific Ultimate 3000 HPLC System using a Macherey-Nagel Nucleodur C18 Gravity column (2 × 50 mm, 1.8 μm) at 0.3 ml/min. The instrument was calibrated in positive and negative mode by direct infusion of a calibration solution (Agilent Technologies ESI-L Low Concentration Tuning Mix). Automated solid phase foldamer synthesis (SPFS) was done via a PurePep Chorus peptide synthesizer from Gyros-Protein Technology with induction heating (see supporting information Scheme S1).

Solid phase synthesis procedures

The protected precursor of oligomer **1** (bearing diethyl phosphonate side chains) was synthesized on Wang resin (0.41 mmol g^{-1}, 30 μmol scale) according to previously reported SPFS protocols (33,34) that were adapted to the PurePep Chorus peptide synthesizer to automatize the foldamer synthesis (35). Monomers with a free carboxylic acid, an Fmoc protected amine, and a protected diethyl phosphonate ester side chain were used and activated as acid chlorides. A typical loading of the first monomer was 0.33 mmol g^{-1} (80%). After purification by preparative and semi-preparative HPLC (C8, 30–70% B, 50°C; A: water + 0.1% TFA, B: acetonitrile + 0.1% TFA), the protected precursor of foldamer **1** was obtained as a light yellow solid (32 mg, 10% yield; HPLC purity: 99%, see Figure S1). HRMS (ESI^+) *m/z* calcd. for $C_{496}H_{579}N_{64}O_{161}P_{32}$: 11004.5348 $(M + H)^+$; found: 2751.6536 $(M + 4H)^{4+}$, 2201.7392 $(M + 5H)^{5+}$, 1834.9627 $(M + 6H)^{6+}$.

Deprotection of ethyl phosphonate oligomer 1

Removal of the diethyl ester protection of the phosphonate side chains (24 mg of protected precursor of foldamer **1**, 2.2 μmol) was carried out following previously described procedures (Scheme S2) (17). After purification by semi-preparative HPLC (C18, 0–100% B, 25°C; A: 12.5 mM TEAA in water pH 8.5, B: 12.5 mM TEAA in water: acetonitrile 1:2 vol/vol pH 8.5) foldamer **1** was obtained as a yellow solid with the side chains as water-soluble triethylammonium phosphonate salts (16 mg, 1.6 μmol, 77%; HPLC purity: 99%, Figure S2). HRMS (ESI^-) *m/z* calcd. for $C_{368}H_{321}N_{64}O_{161}P_{32}$: 9207.0639 $(M\text{-}H)^-$; found: 2300.9965 $(M\text{-}4H)^{4-}$, 1840.7901 $(M\text{-}5H)^{5-}$. On oligomer **1** (11 mg) the exchange of triethylammonium to ammonium cations was performed using Dowex 50W X4 (200–400 Mesh) resin to deliver foldamer **1** with the side chains as water-soluble ammonium phosphonate salts (10 mg). The ^1H NMR spectrum of **1** (Figure S3) matched with that reported previously (17).

Synthesis of biotin-foldamer conjugate 2

N-terminal functionalization of foldamer **1** (5.5 mg, 0.6 μmol) with commercially available biotin-PEG12-OSu reagent was performed following previously reported protocols (Scheme S3) (17). After purification by semi-preparative HPLC (C18, 0–100% B, 25°C; A: 12.5 mM TEAA in water pH 8.5, B: 12.5 mM TEAA in water: acetonitrile 1:2 vol/vol pH 8.5) and the exchange of triethylammonium to ammonium cations, the biotin-foldamer conjugate **2** was obtained as a yellow solid (4.5 mg, 0.45 μmol, 75%; HPLC purity: 98%, Figure S2). HRMS (ESI^-) *m/z* calcd. for $C_{405}H_{388}N_{67}O_{176}P_{32}S$: 10033.0729 $(M-H)^-$; found: 2005.5595 $(M-5H)^{5-}$, 1671.1162 $(M\text{-}6H)^{6-}$. For oligomer **2**, oxidation of the biotin leading to the formation of biotin sulfoxide was observed and characterized by LC-MS spectrometry. HRMS (ESI^-) *m/z* calcd. for $C_{405}H_{388}N_{67}O_{177}P_{32}S$: 10049.0719 $(M-H)^-$; found: 2008.7654 $(M\text{-}5H)^{5-}$, 1673.8154 $(M\text{-}6H)^{6-}$. ^1H NMR (500 MHz, H_2O/D_2O [9:1 vol/vol], 50 mM NH_4HCO_3, water suppression applied at 4.79 ppm which may cause errors in the observed peak intensities in the vicinity of the suppressed peak): δ 11.65 (s), 11.17 (s), 10.47 (s), 10.06 (s), 9.87 (s), 9.82 (s), 9.78 (s), 9.70–9.64 (m), 9.01 (s), 8.83 (s), 8.77 (s), 8.71–8.52 (m), 8.44 (d), 8.32 (d), 8.25 (d), 8.20 (d), 8.14–7.88 (m), 7.77–7.59 (m), 7–56–7.27 (m), 7.18–5.84 (m), 3.79–2.69 (m), 2.16 (t), 1.82–1.71 (m), 1.59–1.5 (m), 1.45–1.35 (m). We have already observed that DNA mimic foldamers and other water-soluble oligoamides mediate biotin oxidation in a length-dependent manner (the longer the foldamer, the faster the oxidation). This is in agreement with literature data (36). The oxidized form of biotin-foldamer conjugate **2** (Figure 1A) could also be used for pull-down experiments. Affinity for streptavidin-functionalized resin beads was sufficient for that purpose. In principle, the oxidation process can be minimized by degassing the solvents before freeze-drying and avoiding exposure of the compound to light.

Preparation of drosophila embryonic extract [DREX]

Drosophila Chromatin Assembly Extract (DREX) was prepared as previously described (6), with minor adjustments. *Drosophila melanogaster* embryos were collected 0–90 min after egg laying and subsequently dechorionated using 3% hypochlorite. The dechorionated embryos were washed in 0.7% NaCl, resuspended in extract buffer (10 mM HEPES [pH 7.6], 10 mM KCl, 1.5 mM $MgCl_2$, 0.5 mM EGTA, 10% glycerol, 10 mM 3-glycero-phosphate; 1 mM dithiothreitol [DTT], and 0.2 mM phenylmethylsulfonyl fluoride [PMSF], added freshly) at 4°C and homogenized using a tight pestle connected to a drill press. The homogenate was supplemented with $MgCl_2$ to a final $MgCl_2$ concentration of 5 mM and centrifuged for 10 min at 10 000 rpm in a SS34 rotor (Sorvall, Thermo-Fisher Scientific, Waltham, USA). The supernatant was centrifuged again for 2 h at 45 000 rpm at 4°C in a SW 56 rotor (Beckman-Coulter, Germany). The clear extract was isolated with a syringe, avoiding the top layer of lipids. Extract aliquots were frozen in liquid nitrogen. Protein concentration was determined by Spectrophotometer (Ds-11, DeNovix, Wilmington, USA) measurement and titration with chromatin assembly experiments.

Plasmids, DNA and primers

PAI61 plasmid (6,10) containing oligomers of sea urchin 5S rDNA nucleosome positioning sequence in pBluescript SK (−) plasmid basic backbone vector. 16 bp control DNA in the interference experiment was obtained by fusing FW: 5′-ATCTAGATCGAGCTACA-3′ and RV: 5′-TGAGCTCGATCTAGAT-3′ primers. The origin plasmid library (28) for nucleosome positioning assays was generated using the S. cerevisiae genomic library (pGP546) from Open Biosystems and expanded as previously described (28,37).

Protein purification

The embryonic *Drosophila melanogaster* histone octamers, INO80 and ORC were expressed and purified as previously described (28,38–42).

SGD chromatin assembly, *in vitro* remodelling assay and MNase–seq

The salt-gradient dialysis (SGD) chromatin and the *in vitro* remodelling assays were performed as described previously (28). Each biological replicate corresponds to a different SGD chromatin preparation and 30 nM ORC and 20 nM INO80 purified from yeast nuclear extracts were used in 100 μl remodelling reactions. The foldamer was titrated against a constant DNA concentration of the SGD chromatin (0.8 μg/100 μl assuming a full assembly) and the following amounts were used: 0.8 μg (1:1), 1.6 μg (1:2), 3.2 μg (1:4) and 6.4 μg (1:8). The sequencing libraries were prepared as before (28) using 10–30 ng mononucleosomal DNA. The samples were diluted to 10 nM, pooled according to the sequencing reads (∼5 million reads per sample), and quantified using the 4150 TapeStation System (Agilent). The pool was sequenced on an Illumina NextSeq1000 in 60 bp paired-end mode (Laboratory for Functional Genome Analysis, Ludwig-Maximilians-Universität Munich). The data processing of the MNase-seq data was done as previously described (28,43,44).

Biotinylation of DNA

Biotinylation of DNA was performed as previously described (6). In short, 500 μg of the pAI61 plasmid was linearized by SacI and XbaI digestion. Subsequently, one end of the DNA was biotinylated by incubation of the linearized DNA with 80 mM dCTP and dGTP, 3 mM biotinylated dUTP and dATP as well as the Klenow Polymerase. The biotinylated DNA was then purified using G50 Sepharose columns (Roche) according to the manufacturer's protocol. Finally, DNA concentration was determined by Spectrophotometer (Ds-11, DeNovix, Wilmington, USA) and adjusted to 200 ng/μl.

Chromatin assembly on immobilized DNA in DREX

2 μg DNA was immobilized on 60 μl M280 paramagnetic streptavidin beads (Invitrogen) in Dynawash buffer (10 mM Tris–HCl [pH 8], 1 M NaCl, 1 mM EDTA) for 1 h. Beads were blocked with BSA (1.75 g/l) for 30 min in EX100, then washed in EX-NP40 (10 mM HEPES pH 7.6, 1.5 mM $MgCl_2$, 0.5 mM EGTA, 10% (v/v) glycerol, 0.05% NP-40). Subsequently, beads were resuspended in a total volume of 240 μl containing 80–160 μl DREX, EX100 buffer (10 mM HEPES [pH 7.6], 100 mM NaCl, 1.5 mM $MgCl_2$, 0.5 mM EGTA, 10% [vol/vol] glycerol; 0.2 mM PMSF, 1 mM DTT, 0.7 μg/ml Pepstatin, 1 μg/ml Aprotinin, 1 μg/ml Leupeptin added fresh), an ATP regenerating system (3 mM ATP, 30 mM creatine phosphate, 10 μg creatine kinase/ml, 3 mM $MgCl_2$ and 1 mM DTT), and free foldamer or 16 bp DNA, depending on the experiment. The assembly reaction was incubated at 26°C for 4 h. After two wash steps with EX200 (10 mM HEPES [pH 7.6], 200 mM NaCl, 1.5 mM $MgCl_2$, 0.5 mM EGTA, 10% [vol/vol] glycerol; 0.2 mM PMSF, 1 mM DTT, 0.7 μg/ml Pepstatin, 1 μg/ml Aprotinin, 1 μg/ml Leupeptin added fresh), beads were prepared for Proteomic Analysis or Micrococcal Nuclease Digestion.

Pulldown with biotinylated foldamer in DREX

1 μg foldamer was immobilized on 30 μl M280 paramagnetic streptavidin beads (Invitrogen) in Dynawash buffer (10 mM Tris–HCl [pH 8], 1 M NaCl, 1 mM EDTA) for 1 h. Beads were blocked with BSA for 30 min (1.75 g/l) in EX100, washed in EX-NP40 (10 mM Hepes pH 7.6, 1.5 mM $MgCl_2$, 0.5 mM EGTA, 10% (v/v) glycerol, 0.05% NP-40) and resuspended in a total volume of 120 μl containing 40–80 μl DREX, EX100 buffer, and ATP regenerating system (3 mM ATP, 30 mM creatine phosphate, 10 μg creatine kinase/ml, 3 mM $MgCl_2$, and 1 mM DTT). The reaction was incubated at 26°C for 1 h, then the beads were prepared for Proteomic Analysis.

Micrococcal nuclease digestion

Chromatin from 2 μg circular DNA assembled for 4 h was resuspended in EX100 containing 5 mM $CaCl_2$ and 100 units/μl of MNase (Sigma). After incubation at room temperature for 30, 60 and 120 s, respectively, a 110 μl fraction of the digestion was stopped by adding 40 μl MNase stop solution (100 mM EDTA [pH 8.0]). The DNA was precipitated and separated with a 1.5% agarose gel upon RNAse A and proteinase K treatment. A Low Molecular weight ladder (New England Biolabs, #N3233S) was used as a size marker.

Sample preparation for proteomic analysis

For assembled chromatin and foldamer pulldowns, the beads-bound fraction was separated by a magnet from the supernatant and washed three times with EX100 and 4 times with fresh 50 mM NH_4HCO_3 to remove detergents and unspecific binders. Tryptic digestion was performed on beads by incubation with 100 μl of 10 ng/μl trypsin (Promega) in 1 M urea 50 mM NH_4HCO_3 for 30 min at 25°C. Beads were separated by a magnet, the supernatant was transferred into a fresh tube, beads were washed twice with 50 mM NH_4HCO_3, and supernatants pooled into the same tube. Supernatant pool was adjusted to final concentration of 1 mM DTT by addition of DTT and digestion was completed overnight at 25°C. Next, the tryptic peptide mixture sample was incubated for 30 min in the dark at 25°C with iodoacetamide at a final concentration of 35 mM to carbamidomethylate sulfhydryl groups of free cysteine. Subsequently, DTT was added to a final concentration of 50 mM and sample was left to incubate for 10 min at 25°C. Then, the sample was acidified using trifluoroacetic acid (TFA), followed by desalting using SDB-RPS (Styrene-divinylbenzene - Reversed Phase Sulfonate, 3M Empore) before mass spectrometry analyses, and redissolved in 15 μl MS loading buffer (Preomics) and stored at −20°C until further processing.

For subcellular fractions were prepared for proteomic analysis using improved sample technology (iST, Preomics) with a SP3 add on (Preomics), following manufacturer's instructions. Afterwards, samples were acidified using trifluoracetic acid (TFA) and underwent a final filtering step over a C8 column, was redissolved in 15μl MS loading buffer (Preomics) and stored at −20°C until further processing.

Cell culture

Drosophila L2–4 cells (45) were grown in Schneider medium supplemented with 10% fetal calf serum, penicillin, and streptomycin at 26°C.

Flow cytometry analysis

Drosophila L2-4 cells were seeded at 1 mio cells/ml in 6-well plates (Sarstedt, Ref: 83.3920), in medium (gibco, Schneider Drosophila medium, Ref: 21720–024) with different concentrations of foldamer (0, 0.01, 0.1, 1, 10 μM) and harvested after 4, 24 or 48 h. Harvested cells were prepared by spinning down of cells at 1000 × g, 4 min and dissolving the pellet in 1 ml PBS. 2.7 ml ice-cold ethanol were added to cell suspension while vortexing. Alcohol-fixed cells were stored stably at 4°C for up to 1 week. On the day of measurement, ethanol was removed by centrifuging cells at 1000 × g for 4 min at 4°C. The supernatant was removed, and cells were resuspended in 1 ml PBS + 1% FBS. Then cells were counted and 0.5×10^6 cells were taken up in 500 μl FACS buffer (PBS + 1% FBS). Finally, 5 μl 100× RNAseA solution in PBS were added to a final concentration of 20 μg/μl. The suspension was incubated 15 min at 37°C, then 50 μl PI stain (10 mg/ml Sigma 1002755458) were added and incubation of 30 min at RT was allowed before measurement. Stained cells were measured using BD LSR-Fortessa (equipped with 405488561633-nm lasers; BD Bioscience), and FlowJo™ v10.8.1 software was used to analyze data.

Subcellular fractionation

Drosophila L2-4 cells were seeded at 1 mio cells/ml in 6 well plates (Sarstedt), in medium (Gibco, Schneider Drosophila medium) with 10 μM foldamer in medium or without foldamer as control and harvested after 48 h. Harvested cells were prepared by spinning down of cells at 1000 × g, 4 min and washing the pellet twice with 2 ml ice cold PBS each. Then, the cells were fractionated using the Subcellular Protein Fractionation Kit for Cultured Cells (Thermo) following the manufacturer's instructions. Adjustments were included for Drosophila cell size, treating the pellet of each well of cells as 5 μl packed cell volume and adjusting buffer volumes accordingly, while also doubling the amount of enzyme and tripling incubation time in MNase digest step. All fractions were stored at −20°C until they were prepared for proteomic analysis.

Proteomic analysis

For LC–MS purposes, desalted peptides were injected in an Ultimate 3000 RSLCnano system (Thermo) and separated in a 25 cm analytical column (75μm ID, 1.6 μm C18, IonOpticks) with a 50 min gradient from 2 to 37% acetonitrile in 0.1% formic acid. The effluent from the HPLC was directly electrosprayed into a Qexactive HF (Thermo) or an Orbitrap Exploris 480 (Thermo) both operated in data-dependent mode to automatically switch between full scan MS and MS/MS acquisition. For Qexactive HF measurements, survey full scan MS spectra (from m/z 375–1600) were acquired with resolution $R = 60\,000$ at m/z 400 (AGC target of 3×10^6). The 10 most intense peptide ions with charge states between 2 and 5 were sequentially isolated to a target value of 1×10^5, and fragmented at 27% normalized collision energy. Typical mass spectrometric conditions were: spray voltage, 1.5 kV; no sheath and auxiliary gas flow; heated capillary temperature, 250ºC; ion selection threshold, 33.000 counts. For Orbitrap Exploris 480 measurements, survey full scan MS spectra (from m/z 350 to 1200) were acquired with resolution $R = 60\,000$ at m/z 400 (AGC target of 3×10^6). The 20 most intense peptide ions with charge states between 2 and 5 were sequentially isolated to a target value of 1×10^5 and fragmented at 30% normalized collision energy. Typical mass spectrometric conditions were as follows: spray voltage, 1.5 kV; heated capillary temperature, 275°C; ion selection threshold, 33 000 counts.

Proteomic data analysis

MaxQuant 1.6.1.5.0 (for *chromatin binders* dataset) or 2.0.1.0 (for *interference proteome* dataset and *foldamer pull-down proteome* dataset) (46) was used to identify proteins and quantify by label free quantification (LFQ) with the following parameters: uniprot_UP000000803_Dmelanogaster _ canonical_isoforms_20200825.fasta (for *chromatin binders* dataset), uniprot-proteome UP000000803_Dmelanogaster _20210818.fasta (for *interference proteome* dataset), Un iprot_AUP000000803_Dmelanosgaster_20211108.fasta (for foldamer pulldown proteome); and Uniprot_UP000000803 _Drome_20220306.fasta (for *subcellular fractionation proteome*). All datasets: MS tol, 10 ppm; MS/MS tol, 20 ppm Da; Peptide FDR, 0.1; Protein FDR, 0.01 min; Peptide Length, 7; Variable modifications, Oxidation (M), Acetyl (Protein N-term); Fixed modifications, Carbamidomethyl (C); Peptides for protein quantitation, razor and unique; Min. peptides, 1; Min. ratio count, 2.

Statistical methods

Data were handled with Perseus software (version 1.6.7.0 and version 2.0.9.0) (47) and R Studio (version 4.0.3). For analysis in Perseus, the output protein_groups.txt file from MaxQuant processing was imported, then protein hits associated with the reversed database, only identified by site and common contaminants were filtered out.

Chromatin binders - three biological replicates of chromatin assembly in DREX on DNA immobilized on beads and beads only control each were acquired and analyzed. All LFQ values were $\log_2(x)$ transformed. Missing values were replaced by random numbers from a standard deviation (width 0.3, downshift 1.8). The two groups (with DNA and beads only) were compared by a two-tailed t-test. Multiple testing correction was applied by using a permutation-based false discovery rate (FDR) method in Perseus. Proteins with an FDR > 0.05 were considered chromatin binders (Figure 1C).

Interference proteome: Three biological replicates for each of the 10 conditions were acquired; each condition

a different concentration of free foldamer or free 16 bp DNA control present during chromatin assembly on beads-immobilized long DNA in DREX. All LFQ values were $\log_2(x)$ transformed. The dataset was filtered strictly so that only proteins with one missing value out of three per condition remained. Then missing values were replaced by random numbers from a standard deviation (width 0.3, downshift 1.8). After, the dataset was matched with the previously mentioned chromatin binder dataset, only proteins that were identified as chromatin binders in the previous dataset remained. The mean of LFQ was determined for each condition. Log_2(LFQ) values of all proteins were normalized to $\log_2$(LFQ) of the lowest concentration of free foldamer/DNA correspondingly. Hierarchical clustering of proteins (rows) based on the distance by Pearson correlation (linkage: average, constraints: none, preprocessed with *k*-means, number of clusters: 300, the maximal number of iterations: 100, restarts: based on values for foldamer conditions revealed two main clusters. Cluster 1 (regarded as proteins that show no interference in binding to chromatin in presence of foldamer) and Cluster 2 (regarded as proteins that show interference in binding to chromatin in presence of foldamer). Sub-clustering of Cluster 2 based on Euclidian distance (linkage: average, constraints: none, preprocessed with k-means, number of clusters: 300, the maximal number of iterations: 100, restarts: revealed sub-clusters 2a (regarded as weak interference) and 2b (regarded as strong interference).

Foldamer pulldown proteome: Three biological replicates, each of biotinylated foldamer immobilized on streptavidin beads, and beads only control, were acquired and analyzed. All LFQ values were $\log_2(x)$ transformed. The dataset was filtered strictly so that only proteins with one missing value out of three per condition remained. Then missing values were replaced by random numbers from a standard deviation (width 0.3, downshift 1.8). The two groups (biotinylated foldamer on beads and beads only) were compared by a two-tailed *t*-test. Multiple testing correction was applied by using a permutation-based false discovery rate (FDR) method in Perseus. Proteins with an FDR > 0.05 were considered foldamer binders (Figure 2B).

GO term analysis for foldamer binders was performed with R Studio version 4.0.3 using the list of identified binders by Perseus, library (org.Dm.eg.db), and Cluster profiler. Enriched GOterms were corrected for semantic redundancy using Cluster Profiler, cutoff 0.6. Only the top eight GOterms were plotted with corresponding p-adjusted values.

Subcellular fractionation proteome: Three biological replicates of 10 μM 48 h foldamer treated and untreated cells were fractionated, acquired and analyzed. All LFQ values were $\log_2(x)$ transformed. The dataset was filtered so that only proteins with at least 2/3 valid values in at least one fraction across both conditions (treated and untreated) remained. Then missing values were replaced by random numbers from a standard deviation (width 0.3, downshift 1.8). For analysis of chromatin-bound fraction, proteins were filtered so that only those with 2/3 valid values before imputation in at least one condition in the chromatin bound fraction (CBE) remained.

Clustering of proteins and visualization for proteomic analysis

Protein Clustering was performed with Cytoscape (version 3.8.2) with string database (version 11.5) plug-in. All nodes represent proteins with at least 1 interaction, only active interaction sources: experimental links, highest confidence interaction score: 0.9, edges based on evidence of interaction, not confidence.

Experimental design and statistical rationale

All assembly experiments were performed in three biological replicates with three independently collected DREX. As negative controls, triplicates of beads only were used. Figure 1B shows an agarose gel as proof of concept. Cell based were performed in 3 biological replicates. A pilot study in our lab revealed that three biological replicates enable us to deduce a precise and statistically valid conclusion between chromatin assembly experiments and the composition of proteins during different time points of assembly.

RESULTS AND DISCUSSION

Foldamer interferes with complex *in vitro* chromatin binding

To investigate whether the foldamers would interfere with *in vitro* chromatin assembly, we incubated linearized and immobilized DNA with a chromatin assembly extract made from early Drosophila embryos (6,48,49) (Figure 1A). The addition of foldamer **1** to the assembly reaction did not interfere with the generation of nucleosomal array ladders, indicating that its presence does not impede general aspects of chromatin assembly such as histone deposition and the formation of regular nucleosomal arrays. A slight reduction in the regularity of the nucleosomal ladder is visible for high foldamer concentrations probably due to the change in protein composition on the fiber (Figure 1B). As the immobilization of the assembled chromatin fiber allowed us to quantify the proteins specifically bound to chromatin (Figure 1C), we could quantify its effect on chromatin composition by adding increasing amounts of foldamer **1** (Figure 1D). Protein intensities for all foldamer concentrations were compared to 1:1 DNA: foldamer mass ratio to prevent bias by DNA-independent effect such as charge density and local pH. The titration experiment revealed two distinct groups or clusters of proteins with regards to their sensitivity towards the foldamer. The first cluster contained proteins that were not affected in their chromatin binding by the presence of the foldamer. This cluster 1 (Cl1) includes the core histones and the HMG-D protein, that can substitute for the linker histone H1, which is absent in preblastoderm embryos of Drosophila (50–52). In addition to the stably bound histones, the chromatin binding of the two large subunits of the histone chaperone Caf-1, the three subunits of the rad50 DNA repair complex, and the heterotrimeric RPA complex are not affected by the presence of the foldamer (Table S1). Interestingly, we also find the two major *Drosophila* topoisomerases (Top3α and Top2) but not Top1, which is competitively inhibited by the foldamer (17,18) in this cluster. The observation

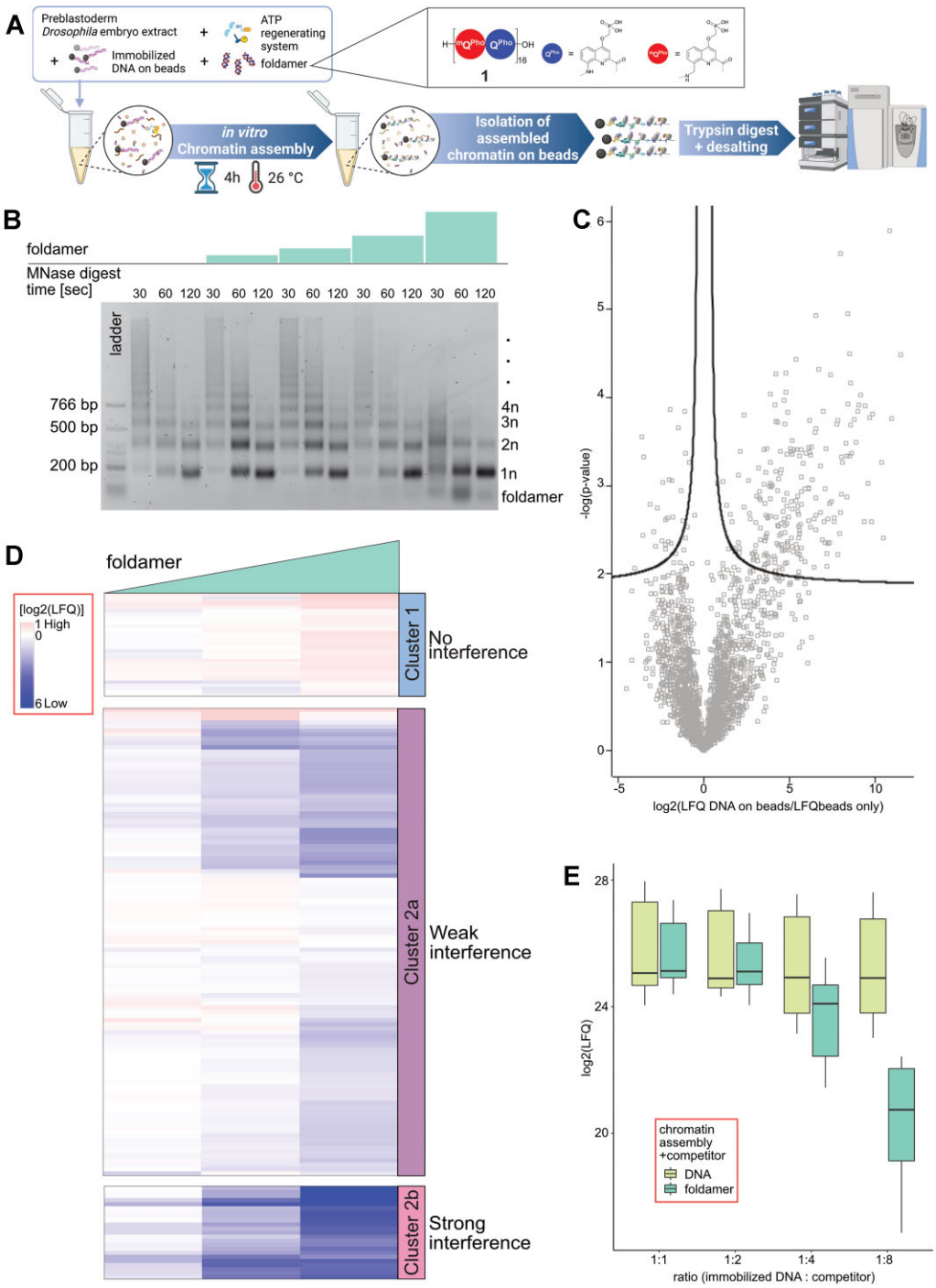

Figure 1. Foldamers interfere with protein binding in DREX-assisted *in vitro* chromatin assembly. (**A**) Schematic diagram of experimental flow for Drosophila embryo extract assisted *in vitro* chromatin assembly. Immobilized DNA on streptavidin beads, ATP generating system, and foldamer **1** (inset panel depicts chemical structure of DNA mimic foldamer **1** and formulae of amino acid monomers Q^{Pho} (blue) and $^{m}Q^{Pho}$ (red)) were added to DREX extract, incubated for 4 h at 26°C, then assembled chromatin was isolated, washed, and prepared for mass spectrometry measurement. (**B**) Agarose gel of Mnase digested chromatin assemblies in absence of foldamer **1** or in presence of 1, 2, 4 or 8 equivalents of foldamer **1** compared to DNA. Labelling reflects nucleosomal ladder containing a regular array of nucleosomes (1n/2n/3n/4n…) as well as a band of residual free foldamer. (**C**) Volcano plot for proteins enriched on biotinylated DNA bound to beads over beads only control after 4 h incubation in DREX extract in absence of foldamer **1**. $N = 3$ FDR = 0.05. (**D**) Heatmap of proteins binding to DNA fiber during chromatin assembly (rows) against their mean intensities at different concentrations of free foldamer present (columns). Unbiased Pearson clustering results in two groups: proteins whose binding is not interfered with by foldamer **1**: 'No interference (Cluster1)' (blue) and interfered by foldamer **1** 'Interference (Cluster2)'. Subsequent Euclidian clustering separates Cluster 2 into Cluster 2a 'weak interference' (dark purple) and Cluster 2b 'strong interference' (pink).' The DNA: foldamer **1** weight ratio ranged between 1:1 to 1:8. $N = 3$. (**E**) Boxplot of chromatin binding of proteins belonging to the origin recognition complex ORC 1–5, all located in Cluster 2b 'strong interference'. Titration of chromatin binding using foldamer **1** (turquoise) or free 16 bp DNA control (lime green) as competitors. Each box consists of the $N = 3$ technical replicates of all 5 proteins.

that the different topoisomerases have different sensitivities towards the foldamer further supports previous findings of some structural specificity of the foldamer. For proteins of Cl1, the lack of effect of the foldamer may reflect inherently stronger binding of these proteins to the long, immobilized DNA than to the foldamer. Alternatively, binding of those proteins to chromatin may at least be partially mediated by foldamer-resistant protein–protein rather than protein–DNA interactions.

The second cluster of 138 proteins, which could be further subdivided into sub-clusters 2a and b, contained proteins that were either mildly (Cl2a) or strongly (Cl2b) affected by increasing amounts of foldamer (Figure 1D, Table S1). The 115 proteins that were affected mildly by foldamer (Cl2a) contained a lot of bona fide chromatin-associated factors such as subunits of the condensin and cohesion complex, several structural proteins, and multiple proteins involved in various forms of DNA repair (52). This enrichment of DNA repair factors on linearized chromatin has been reported before (48). The interference experiment now enables us to identify the factors that bind chromatin by recognising structural features of double-stranded DNA. While interference with the proteins in cluster 2a was only mild, the 23 proteins in cluster 2b were affected much more by increasing foldamer concentrations. This strong effect of the foldamer suggests that the chromatin binding of these proteins is largely mediated by their interaction with short stretches of DNA in a non-sequence-specific manner. In fact, the effect of foldamer addition is much stronger than the one of a DNA double helix of similar length (Figure 1E). Interestingly, cluster 2b contains almost all subunits of the origin recognition complex (ORC) and several subunits of the Sin3A transcriptional repressor complex. Our findings of different sensitivities of chromatin interacting proteins towards the presence of foldamer underscore the importance of studying the effect of such foldamers in the context of complex chromatin rather than on isolated proteins.

The foldamer interaction proteome

To identify the proteins and protein complexes that bind directly to the foldamer, we analysed the foldamer-bound proteome from the same Drosophila early embryonic extracts that we have used to assemble chromatin *in vitro* (Figure 2A). To do this, biotinylated foldamer **2** (Figure 2A) was immobilized on magnetic beads and used as an affinity reagent. LC-MS analysis of the specifically bound proteins revealed 640 proteins as specific foldamer interactors (Figure 2B, Table S2). The fact that we find more specific foldamer binders than proteins bound to assembled chromatin, supports the hypothesis that the chromatin structure has evolved to limit the interactions between proteins and the polyanionic DNA in eukaryotes (53). The foldamer-bound proteome contains a large number of proteins annotated as binders of double-stranded nucleic acids, underscoring the successful design of the molecule as a DNA mimic (Figure 2C and D). As a confirmation of earlier findings, the previously characterized foldamer target protein topisomerase1 (Top1) appears as a specific binder (17,18). However, we also find many other known DNA binders such as the basal transcription machinery or sequence-specific transcription factors containing Zn-finger domains in the foldamer-bound proteome. The latter comes as a surprise for the reasons mentioned in the introduction: the foldamer lacks the sequence features that transcription factors normally recognize. This presumably reflects the fact that sequence-selective DNA-binding proteins also have a certain sequence independent affinity through interaction with the B-form DNA. In addition, we also detect known RNA-binding proteins in the foldamer pulldowns, although the foldamer structure has not been designed to resemble double stranded RNAs as found in stem loop structures. A good example of this is the presence of several known components of the spliceosome and many ribosomal factors in the foldamer pulldown in addition to other factors that carry RNA binding domains (Figure 2C and D, Table S2). We compared the foldamer interactome of the foldamer **1**, corresponding to 16bp DNA and used throughout the rest of this study, with the interactome of a foldamer of half its length (8bp) (Figure S4). The proteins detected show similar degrees of enrichment over beads only control with a slight bias for better binding to the longer foldamer. Altogether, the results from pull-down experiments and interference with chromatin assembly show the differential impact foldamer has on complex systems and provide a large amount of information that can be used as starting points for more advanced investigation.

ORC complex gets competed off fibre by binding directly to foldamers

Studying the effect of foldamers on chromatin assembly or their ability to pull down proteins from complex embryo extracts is more physiological than investigating their effect on isolated proteins. However, due to its limitations in absolute quantification neither the competition experiment nor the binding study alone allowed us to immediately derive a hypothesis about the potential effect of foldamers on living cells. The observed inhibition of protein binding to chromatin by the foldamer might as well be an indirect and potentially artificial effect. In other words, the interaction of a given protein with the foldamer may not necessarily result in an interference with its function *in vivo*. To identify proteins where the interference with chromatin binding is mediated by an interaction with the foldamer, we compared the results of both experiments. This led to the identification of 15 proteins that fulfilled these criteria in our subset (Figure 2E). These 15 proteins were predominantly involved in DNA replication and DNA damage control. Most strikingly, the set contained the ORC core complex known to bind replication origins. The canonical function of ORC is to bind to replication origins to recruit and load, in cooperation with Cdc6, the replication helicase (Cdt1-MCM) in the G1-phase of cell division (54). The pull-down of ORC hints at a direct binding to the foldamer and thus suggests that such binding is what caused the premature dissociation of ORC from chromatin fibres when they assemble in presence of the foldamer.

The addition of foldamer interferes with ORC's dependant generation of nucleosomal arrays at origins

To investigate the functional impact of the foldamer through interference with ORC binding, we tested the

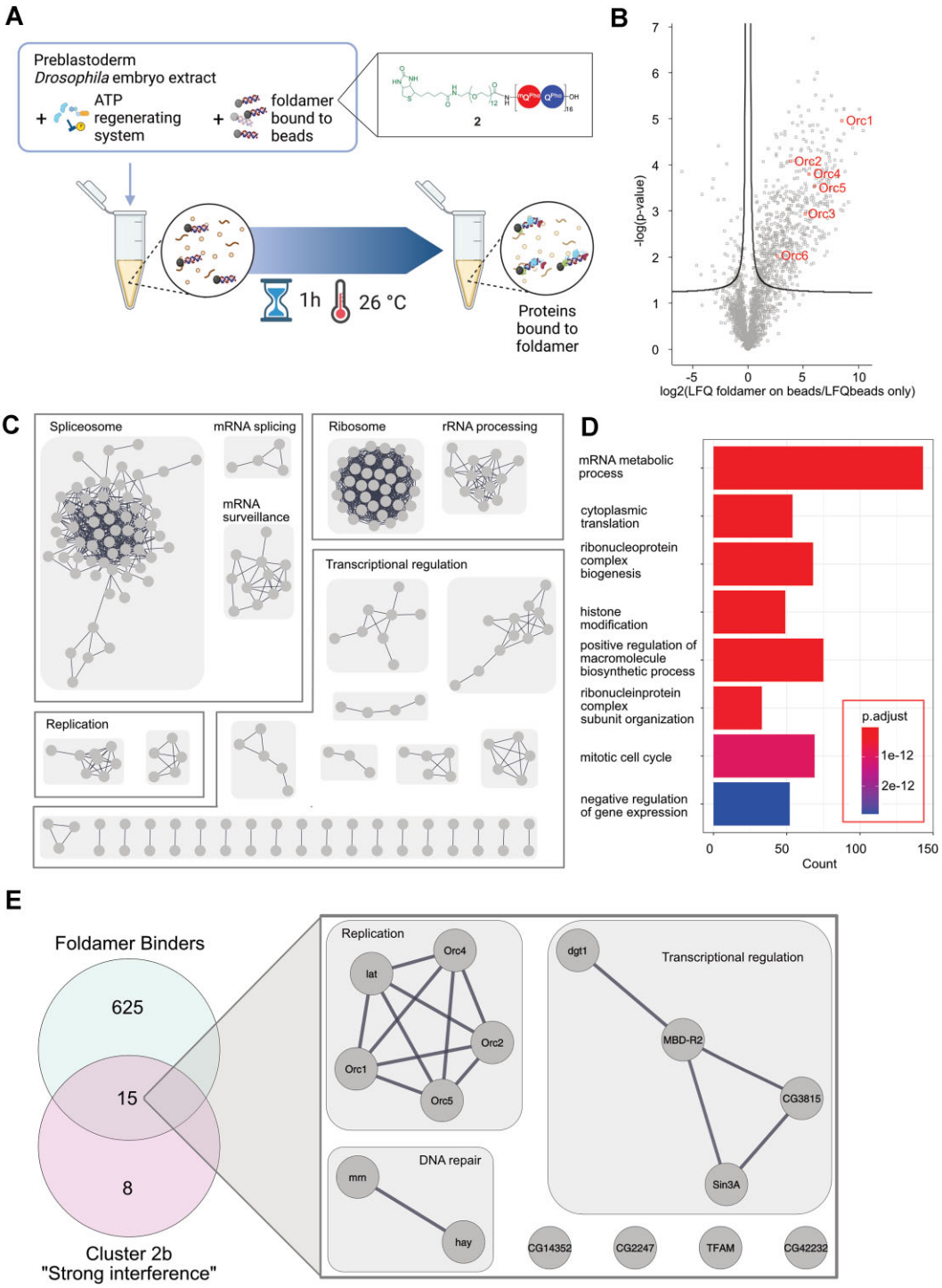

Figure 2. Identification and characterization of proteins susceptible to foldamer binding and comparison to the competition experiment. (**A**) Schematic diagram of experimental flow of foldamer pulldown from preblastoderm Drosophila embryo extract (DREX) with foldamer **2** (Structure displayed in inset panel: Foldamer **2** is functionalized at the N-terminus with biotin (green)). (**B**) Volcano plot for Pulldown of proteins with 1 μg biotinylated foldamer from DREX. Orc subunits are highlighted in red. $N = 3$ FDR $= 0.05$. (**C**) Cytoscape network plot after string analysis (only experimental links, highest confidence interaction score 0.9) for proteins binding to biotinylated foldamer in DREX. (**D**) Top 8 GO Terms by p-value for all proteins specifically binding to biotinylated foldamer in DREX. (**E**) Comparison of proteins binding foldamer to proteins interfered in binding of chromatin fiber in presence of foldamer. Venn diagram depicting the overlap of the two sets. Cytoscape network plot after string analysis (only experimental links, highest confidence interaction score 0.9) for proteins shown to be binding to foldamer and interfered with strongly by foldamer in chromatin assembly in DREX.

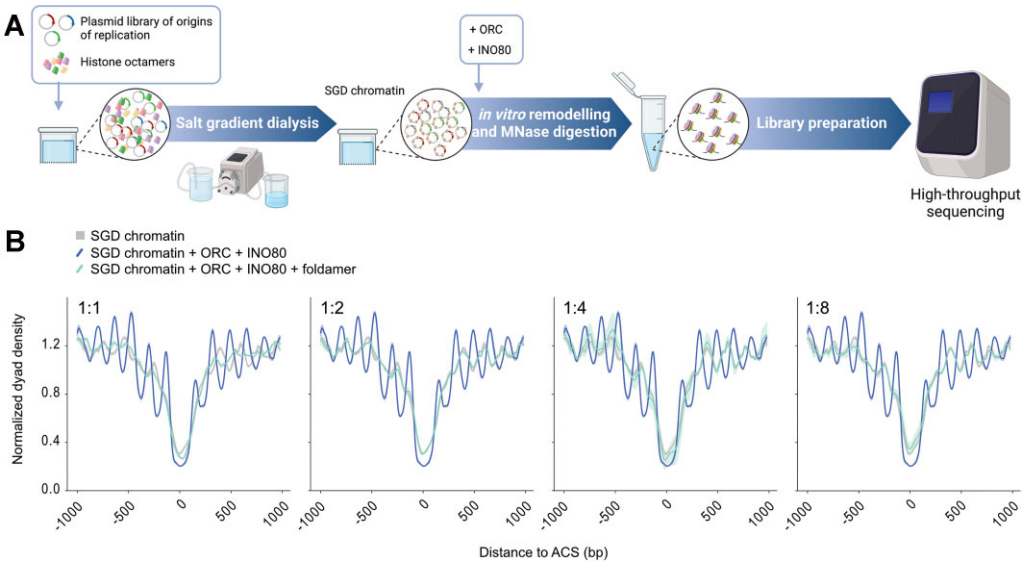

Figure 3. Foldamer interferes with the chromatin remodelling activity of ORC at origins of replication. (**A**) Schematic diagram of experimental flow of *in vitro* functional assay. (**B**) Averaged composite plots of biological replicates including the standard error (s.e.m.) of *in vitro* MNase-seq data for SGD chromatin (grey, n = 2) incubated with INO80 and ORC without (dark blue, $n = 2$) or with foldamer (turquoise, $n = 2$). Ratio on top of each plot indicates DNA : foldamer (w:w) ratio assuming a full assembly of the SGD chromatin. Sequencing reads were aligned to the ACS, the ORC-binding motif.

ability of ORC to induce the formation of regular nucleosomal arrays around yeast origins in the presence of foldamer (Figure 3A). A functional ORC and remodelling complex INO80 is essential to orchestrate remodelers to form flanking nucleosomal arrays around replication origins (28). Purified yeast ORC and INO80 proteins were incubated with chromatin assembled by salt gradient dialysis on a library containing around 300 yeast origins as previously described (28) and with increasing amounts of foldamer. The formation of regular nucleosomal arrays around these origins was then analysed by MNase-seq. In presence of foldamer, nucleosomal arrays were not generated, showing that, independently of the species used, the foldamer interferes with the organization around chromatin around replication origins (Figure 3B).

Foldamer treatment also disturbs the chromatin-bound proteome in S2 drosophila tissue culture cells

To confirm the effect of the foldamer on the chromatin-bound proteome *in vivo*, we treated S2 Drosophila cells with 10 μM foldamer for 48h. In earlier studies, it was shown that the foldamers may not readily enter cells because of their polyanionic nature and that some carrier would be needed for in-cell delivery (17). However, we have observed that Drosophila S2 cells easily absorb foldamer even without the addition of a carrier, which had also been shown before for other large polyanions (55). Subsequent subcellular fractionation and proteomic analysis allowed us to follow protein distribution upon foldamer treatment (Figure 4A). Consistent with its DNA mimicking properties, we found that overall protein intensity in the chromatin-bound fraction decreased after foldamer treatment (Figure 4B). Analysis of the intensities of proteins found on chromatin during *in vitro* assembly (Figure 1C) showed a similar behavior towards foldamer treatment (Figure 4C). In cluster 1, chromatin binding is maintained upon foldamer treatment, whereas we see a mild downshift trend for Cluster 2a and a significantly stronger downshift in protein intensity for Cluster2b. The histone proteins for example remain bound to chromatin upon foldamer treatment whereas the chromatin binding of the detected ORC proteins is substantially reduced (Figure 4D). Overall, this experiment not only validates the clustering of proteins based on their response to the presence of the foldamer *in vitro*, but it also shows that the proteins are affected similarly in cells.

Foldamer treatment interferes with cell cycle progression

We report a significant impact on chromatin binding of ORC *in vitro* and *in vivo* and show a loss of its function at replication origins *in vitro*. We, therefore, wondered whether the addition of the foldamer would also interfere with cell cycle progression *in vivo*. Hence, we exposed Drosophila S2 cells to a medium containing different concentrations of foldamer **1** (0, 0.01, 0.1, 1, 10 μM) for 4, 24 or 48 h (Figure 5A). Flow cytometry after propidium iodide staining revealed a time and concentration-dependent effect of the foldamer on the cell cycle stages of the treated cells (Figure 5B and C, Figure S5 and Table S3). The ratio of cells in S-Phase increased for 10 μM foldamer concentration to 15% (versus 10% in untreated control) after 24 h and even significantly high to 33% (versus 11% in untreated control) after 48 h (Figure 5C, Table S3). A similar, yet weaker, trend can be seen for a concentration of 1 μM foldamer in medium. S-Phase arrest has been observed before when Orc function of setting up chromatin structure is impaired (28). Our findings show that foldamers disturbs the cell cycle, putatively through direct interactions with the ORC complex resulting in an interference with its chromatin binding thereby blocking cell cycle progression.

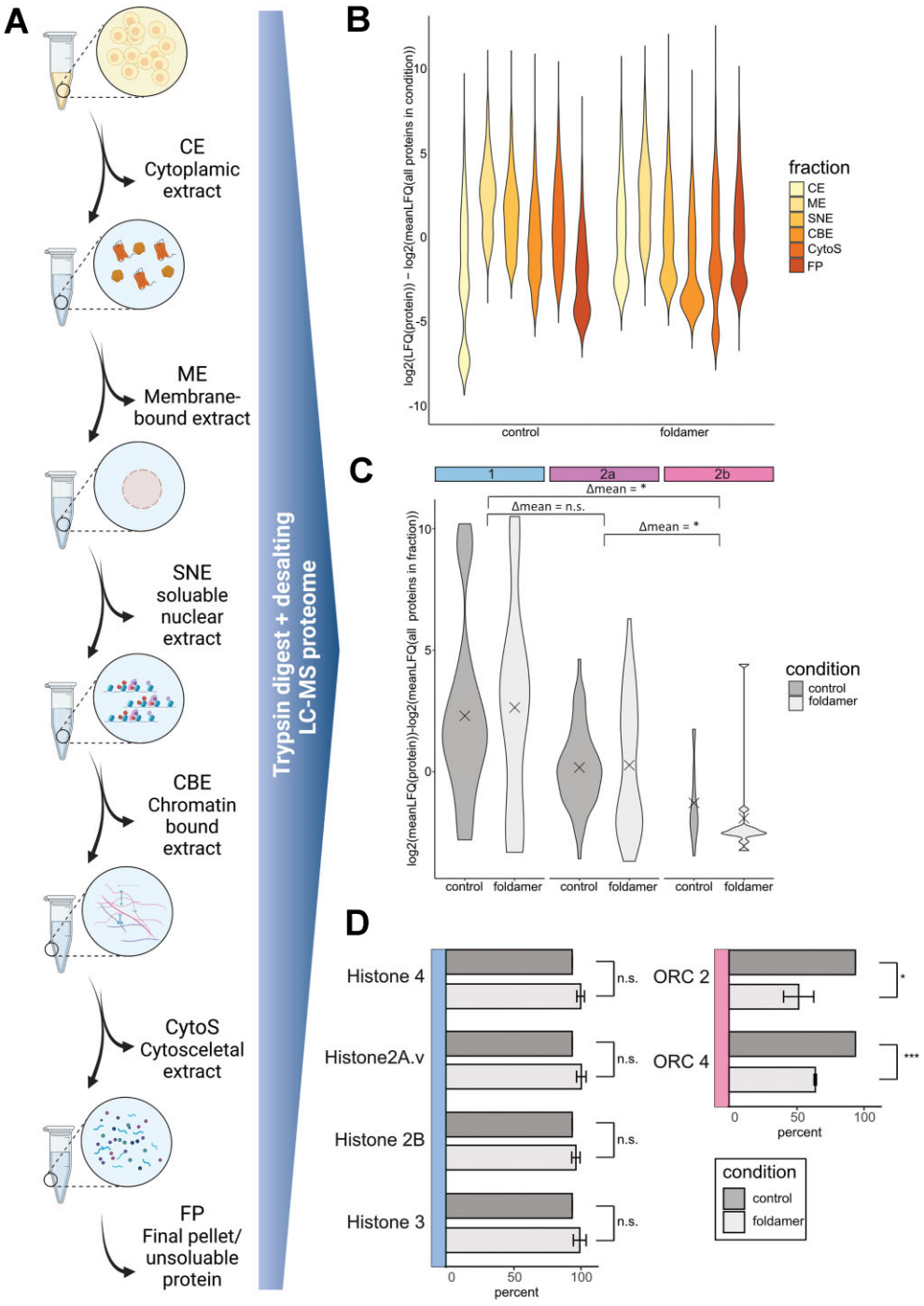

Figure 4. Subcellular fractionation of Drosophila cells confirms *in vitro* data on effect of foldamer on chromatin-bound proteins. (**A**) Schematic diagram of experimental flow of subcellular fractionation experiment. (**B**) Violin plot of mean protein intensities in the subcellular fractions in control and upon treatment with 10μM foldamer **1**. Cross marks mean value in fraction, Number of proteins = 3765. $N = 3$. (**C**) Violin plot of means of protein intensities in CBE (chromatin-bound) fraction of the proteins appearing in clusters **1**, **2a** and **2b** as defined by their sensitivity to foldamer *in vitro*. Cross marks indicate mean value. Statistics describe comparison of the mean differences of all proteins in each group with $N = 3$ replicates $^{*}P < 0.05$, one-way ANOVA + Tukey's test. (**D**) Bar graph of foldamer effect on protein intensity of selected proteins in chromatin-bound fraction (CBE). $N = 3$ replicates $^{**}P < 0.01$, $^{***}P < 0.001$, *t*-test.

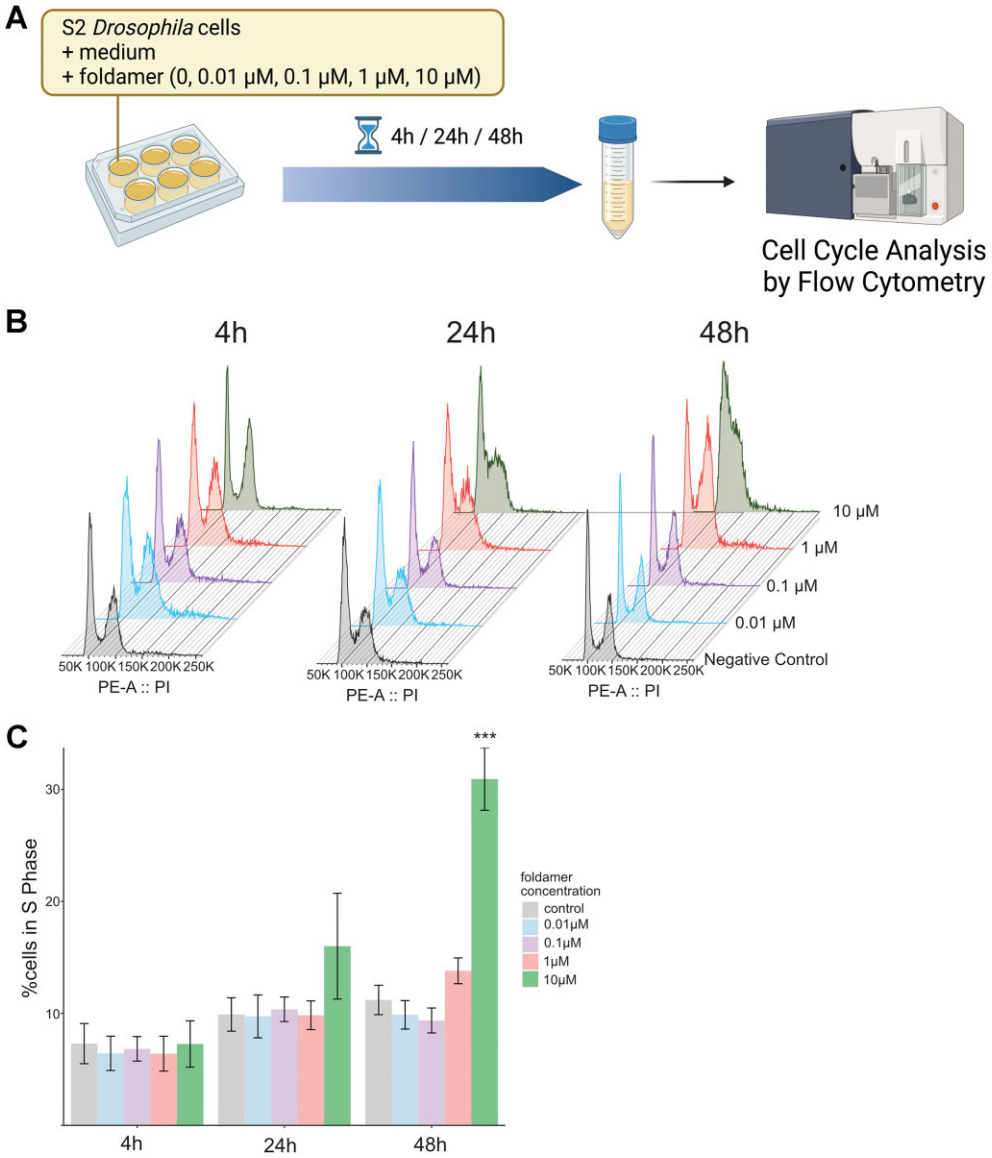

Figure 5. Foldamer leads to accumulation of cells in S-Phase *in vivo*. (**A**) Schematic diagram of experimental flow of cell cycle analysis experiment. (**B**) Representative cell cycle profiles after 4, 24 and 48 h of treatment with different concentrations of foldamer **1** in serum, determined by flow cytometry with PI stain. (**C**) Bar graph representing percentage of cells in S-Phase after foldamer treatment with indicated concentration after the indicated time. Error bars represent standard deviation, $N = 3$ replicates $^{***}P < 0.001$ against all other values in the group, one-way ANOVA + Tukey's test.

CONCLUSION

The chromatin-bound proteome plays an important role in the interpretation of genetic information and is involved in setting up cell type and tissue-specific epigenomes. Considering that many proteins bind chromatin not only by recognizing DNA through its sequence but also its shape or in combination with other proteins, the use of rationally designed stable DNA mimic foldamers is a powerful new method to selectively target those interactions. So far, most investigations had been performed on isolated DNA binding molecules in presence of isolated DNA substrates (17,18), which is far from being physiological. In the eukaryotic nucleus, DNA is packaged in chromatin, which is a highly complex and dynamic structure containing multiple proteins competing for interactions (4,5). To better resemble the *in vivo* situation, we therefore used a complex *in vitro* chromatin assembly system from Drosophila preblastoderm embryos. This allowed us to identify the most likely targets of the foldamers *in vivo*. One of the strongest targets of foldamer turned out to be the highly conserved ORC complex. ORC is essential for DNA replication and has recently been shown to act as a major organiser of chromatin structure around replication origins together with the nucleosome remodelling complex INO80 (28). We show this function is greatly disturbed when foldamer is present and results in a block of S-Phase progression upon foldamer treatment. Our experiments demonstrate the power of using complex *in vitro* systems to investigate multi-factorial biological processes such as chromatin assembly and binding. Combined with proteomics, this approach constitutes a

novel and efficient way to rapidly investigate the pleiotropic effects of DNA mimics on chromatin and correctly predict their effect *in vivo*.

DATA AVAILABILITY

Proteomic data have been deposited to the ProteomeXchange Consortium via the PRIDE partner repository with the dataset identifiers: PXD039966 (Drosophila embryo extract assisted *in vitro* chromatin assembly in presence of 16mer foldamer), PXD040158 (DNA mimicking 32mer foldamers interfere with *in vitro* chromatin assembly in Drosophila embryo extract), PXD040157 (Pulldown with DNA mimicking foldamers in preblastoderm Drosophila embryo extract) and PXD042288 (Subcellular fractionation of Drosophila S2 cells upon foldamer treatment). The raw and processed files from the high-throughput sequencing data (MNase-seq) have been deposited in the National Center for Biotechnology Information (NCBI) Gene Expression Omnibus (GEO) with the accession number GSE236969.

SUPPLEMENTARY DATA

Supplementary Data are available at NAR Online.

ACKNOWLEDGEMENTS

We would like to thank the entire Imhof and Huc laboratory members for their lively discussions and constant support. We thank Anuroop V. Venkatasubramani and Nikolas Eggers for their assistance in visualization of the data. All schematic figures were created with BioRender.com. We also thank H. Blum and S. Krebs (LAFUGA) for high-throughput sequencing.

FUNDING

V.K. is supported by the grants of the Deutsche Forschungsgemeinschaft (DFG) [194407719 (QBM) and 213249687 (CRC1064)]; DFG [213249687 (CRC1064) to A.I. and C.F.K. and 325871075 (CRC1309) to A.I.]; D.B.K. received funding from the European Union's Framework Programme for Research and Innovation Horizon 2020 (2014–2020) under the Marie Skłodowska-Curie Grant [754388]; LMU Munich's Institutional Strategy LMUexcellent within the framework of the German Excellence Initiative [ZUK22]; work in the I.H. lab was supported by the DFG [HU1766/2-1 and 325871075 (CRC1309-C7)]; European Research Council (ERC) under the European Union's Horizon Europe Framework Programme [ERC-2021-ADG-320892]. Funding for open access charge: Deutsche Forschungsgemeinschaft (DFG).
Conflict of interest statement. None declared.

REFERENCES

1. Campos,E.I. and Reinberg,D. (2009) Histones: annotating chromatin. *Annu. Rev. Genet.*, **43**, 559–599.
2. Dai,Z., Ramesh,V. and Locasale,J.W. (2020) The evolving metabolic landscape of chromatin biology and epigenetics. *Nat. Rev. Genet.*, **21**, 737–753.
3. Cai,S.F., Chen,C.-W. and Armstrong,S.A. (2015) Drugging chromatin in cancer: recent advances and novel approaches. *Mol. Cell*, **60**, 561–570.
4. Kustatscher,G., Hégarat,N., Wills,K.L.H., Furlan,C., Bukowski-Wills,J.-C., Hochegger,H. and Rappsilber,J. (2014) Proteomics of a fuzzy organelle: interphase chromatin. *EMBO J.*, **33**, 648–664.
5. Aranda,S., Alcaine-Colet,A., Blanco,E., Borràs,E., Caillot,C., Sabido,E. and Croce,L.D. (2019) Chromatin capture links the metabolic enzyme AHCY to stem cell proliferation. *Sci. Adv.*, **5**, eaav2448.
6. Völker-Albert,M.C., Pusch,M.C., Fedisch,A., Schilcher,P., Schmidt,A. and Imhof,A. (2016) A quantitative proteomic analysis of in VitroAssembled chromatin. *Mol. Cell Proteomics*, **15**, 945–959.
7. Rafiee,M.-R., Girardot,C., Sigismondo,G. and Krijgsveld,J. (2016) Expanding the circuitry of pluripotency by selective isolation of chromatin-associated proteins. *Mol. Cell*, **64**, 624–635.
8. Sirbu,B.M., Couch,F.B. and Cortez,D. (2012) Monitoring the spatiotemporal dynamics of proteins at replication forks and in assembled chromatin using isolation of proteins on nascent DNA. *Nat. Protoc.*, **7**, 594–605.
9. Alabert,C., Bukowski-Wills,J.-C., Lee,S.-B., Kustatscher,G., Nakamura,K., Alves,F.d.L., Menard,P., Mejlvang,J., Rappsilber,J. and Groth,A. (2014) Nascent chromatin capture proteomics determines chromatin dynamics during DNA replication and identifies unknown fork components. *Nat. Cell Biol.*, **16**, 281–293.
10. Nakamura,K., Kustatscher,G., Alabert,C., Hödl,M., Forne,I., Völker-Albert,M., Satpathy,S., Beyer,T.E., Mailand,N., Choudhary,C. *et al.* (2021) Proteome dynamics at broken replication forks reveal a distinct ATM-directed repair response suppressing DNA double-strand break ubiquitination. *Mol. Cell*, **81**, 1084–1099.
11. Weickert,P., Li,H.-Y., Götz,M.J., Dürauer,S., Yaneva,D., Zhao,S., Cordes,J., Acampora,A.C., Forne,I., Imhof,A. *et al.* (2023) SPRTN patient variants cause global-genome DNA-protein crosslink repair defects. *Nat. Commun.*, **14**, 352.
12. Lyon,A.S., Peeples,W.B. and Rosen,M.K. (2021) A framework for understanding the functions of biomolecular condensates across scales. *Nat. Rev. Mol. Cell Biol.*, **22**, 215–235.
13. Gibson,B.A., Doolittle,L.K., Jensen,L.E., Gamarra,N., Redding,S. and Rosen,M.K. (2019) Organization and regulation of chromatin by liquid-liquid phase separation. *Cell*, **179**, 470–484.
14. Stewart-Morgan,K.R., Petryk,N. and Groth,A. (2020) Chromatin replication and epigenetic cell memory. *Nat. Cell Biol.*, **22**, 361–371.
15. Polo,S.E. and Almouzni,G. (2015) Chromatin dynamics after DNA damage: the legacy of the access-repair-restore model. *DNA Repair (Amst.)*, **36**, 114–121.
16. Raschle,M., Smeenk,G., Hansen,R.K., Temu,T., Oka,Y., Hein,M.Y., Nagaraj,N., Long,D.T., Walter,J.C., Hofmann,K. *et al.* (2015) Proteomics reveals dynamic assembly of repair complexes during bypass of DNA cross-links. *Science*, **348**, 1253671.
17. Ziach,K., Chollet,C., Parissi,V., Prabhakaran,P., Marchivie,M., Corvaglia,V., Bose,P.P., Laxmi-Reddy,K., Godde,F., Schmitter,J.-M. *et al.* (2018) Single helically folded aromatic oligoamides that mimic the charge surface of double-stranded B-DNA. *Nat. Chem.*, **10**, 511–518.
18. Corvaglia,V., Carbajo,D., Prabhakaran,P., Ziach,K., Mandal,P.K., Santos,V.D., Legeay,C., Vogel,R., Parissi,V., Pourquier,P. *et al.* (2019) Carboxylate-functionalized foldamer inhibitors of HIV-1 integrase and topoisomerase 1: artificial Analogues of DNA mimic proteins. *Nucleic Acids Res.*, **47**, 5511–5521.
19. Wang,H.C., Chou,C.C., Hsu,K.C., Lee,C.H. and Wang,A.H.J. (2019) New paradigm of functional regulation by DNA mimic proteins: recent updates. *IUBMB Life*, **71**, 539–548.
20. Wang,H.-C., Ho,C.-H., Hsu,K.-C., Yang,J.-M. and Wang,A.H.J. (2014) DNA mimic proteins: functions, structures, and bioinformatic analysis. *Biochemistry*, **53**, 2865–2874.
21. Bando,T. and Sugiyama,H. (2006) Synthesis and biological properties of sequence-specific DNA-alkylating pyrrole−imidazole polyamides. *Acc. Chem. Res.*, **39**, 935–944.
22. Dervan,P.B. and Edelson,B.S. (2003) Recognition of the DNA minor groove by pyrrole-imidazole polyamides. *Curr. Opin. Struct. Biol.*, **13**, 284–299.
23. Chenoweth,D.M., Poposki,J.A., Marques,M.A. and Dervan,P.B. (2007) Programmable oligomers targeting 5′-GGGG-3′ in the minor

groove of DNA and NF-κb binding inhibition. *Bioorg. Med. Chem.*, **15**, 759–770.
24. Janssen,S., Durussel,T. and Laemmli,U.K. (2000) Chromatin opening of DNA satellites by targeted sequence-specific drugs. *Mol. Cell*, **6**, 999–1011.
25. Blattes,R., Monod,C., Susbielle,G., Cuvier,O., Wu,J.-h., Hsieh,T.-s., Laemmli,U.K. and Käs,E. (2006) Displacement of D1, HP1 and topoisomerase II from satellite heterochromatin by a specific polyamide. *EMBO J.*, **25**, 2397–2408.
26. Janssen,S., Cuvier,O., Müller,M. and Laemmli,U.K. (2000) Specific gain- and loss-of-function phenotypes induced by satellite-specific DNA-binding drugs fed to Drosophila melanogaster. *Mol. Cell*, **6**, 1013–1024.
27. Kopytova,D., Popova,V., Kurshakova,M., Shidlovskii,Y., Nabirochkina,E., Brechalov,A., Georgiev,G. and Georgieva,S. (2016) ORC interacts with THSC/TREX-2 and its subunits promote Nxf1 association with mRNP and mRNA export in Drosophila. *Nucleic Acids Res.*, **44**, 4920–4933.
28. Chacin,E., Reusswig,K.-U., Furtmeier,J., Bansal,P., Karl,L.A., Pfander,B., Straub,T., Korber,P. and Kurat,C.F. (2023) Establishment and function of chromatin organization at replication origins. *Nature*, **616**, 836–842.
29. Remus,D., Beall,E.L. and Botchan,M.R. (2004) DNA topology, not DNA sequence, is a critical determinant for Drosophila ORC–DNA binding. *EMBO J.*, **23**, 897–907.
30. Vashee,S., Cvetic,C., Lu,W., Simancek,P., Kelly,T.J. and Walter,J.C. (2003) Sequence-independent DNA binding and replication initiation by the human origin recognition complex. *Genes Dev.*, **17**, 1894–1908.
31. Prioleau,M.-N. and MacAlpine,D.M. (2016) DNA replication origins—where Do we begin?*Genes Dev.*, **30**, 1683–1697.
32. Kuo,A.J., Song,J., Cheung,P., Ishibe-Murakami,S., Yamazoe,S., Chen,J.K., Patel,D.J. and Gozani,O. (2012) The BAH domain of ORC1 links H4K20me2 to DNA replication licensing and Meier-Gorlin syndrome. *Nature*, **484**, 115–119.
33. Baptiste,B.t., Douat-Casassus,C.l., Laxmi-Reddy,K., Godde,F.d. and Huc,I. (2010) Solid phase synthesis of aromatic oligoamides: application to helical water-soluble foldamers. *J. Org. Chem.*, **75**, 7175–7185.
34. Hu,X., Dawson,S.J., Nagaoka,Y., Tanatani,A. and Huc,I. (2016) Solid-phase synthesis of water-soluble helically folded hybrid α¯amino acid/quinoline oligoamides. *J. Org. Chem.*, **81**, 1137–1150.
35. Corvaglia,V., Sanchez,F., Menke,F.S., Douat,C. and Huc,I. (2023) Optimization and automation of helical aromatic oligoamide foldamer solid-phase synthesis. *Chem. Eur. J.*, **29**, e202300898.
36. Rebhan,M.A.E., Brunschweiger,A. and Hall,J. (2013) Measurement by SPR of very low dissociation rates: oxidation-mediated loss of biotin–Streptavidin affinity. *ChemBioChem*, **14**, 2091–2094.
37. Jones,G.M., Stalker,J., Humphray,S., West,A., Cox,T., Rogers,J., Dunham,I. and Prelich,G. (2008) A systematic library for comprehensive overexpression screens in Saccharomyces cerevisiae. *Nat. Meth.*, **5**, 239–241.
38. Simon,R.H. and Felsenfeld,G. (1979) A new procedure for purifying histone pairs H2A + H2B and H3 + H4 from chromatin using hydroxylapatite. *Nucleic Acids Res.*, **6**, 689–696.
39. Krietenstein,N., Wippo,C.J., Lieleg,C. and Korber,P. (2012) Genome-wide in vitro reconstitution of yeast chromatin with in vivo-like nucleosome positioning. *Meth. Enzymol.*, **513**, 205–232.
40. Shen,X. (2004) Preparation and analysis of the INO80 complex. *Meth. Enzymol.*, **377**, 401–412.
41. Kurat,C.F., Yeeles,J.T.P., Patel,H., Early,A. and Diffley,J.F.X. (2017) Chromatin controls DNA replication origin selection, lagging-strand synthesis, and replication fork rates. *Mol. Cell*, **65**, 117–130.
42. Frigola,J., Sabarinathan,R., Mularoni,L., Muiños,F., Gonzalez-Perez,A. and López-Bigas,N. (2017) Reduced mutation rate in exons due to differential mismatch repair. *Nat. Genet.*, **49**, 1684–1692.
43. Oberbeckmann,E., Niebauer,V., Watanabe,S., Farnung,L., Moldt,M., Schmid,A., Cramer,P., Peterson,C.L., Eustermann,S., Hopfner,K.-P. *et al.* (2021) Ruler elements in chromatin remodelers set nucleosome array spacing and phasing. *Nat. Commun.*, **12**, 3232.
44. Oberbeckmann,E., Krietenstein,N., Niebauer,V., Wang,Y., Schall,K., Moldt,M., Straub,T., Rohs,R., Hopfner,K.-P., Korber,P. *et al.* (2021) Genome information processing by the INO80 chromatin remodeler positions nucleosomes. *Nat. Commun.*, **12**, 3231.
45. Thomae,A.W., Schade,G.O.M., Padeken,J., Borath,M., Vetter,I., Kremmer,E., Heun,P. and Imhof,A. (2013) A pair of centromeric proteins mediates reproductive isolation in drosophila species. *Dev. Cell*, **27**, 412–424.
46. Tyanova,S., Temu,T. and Cox,J. (2016) The MaxQuant computational platform for mass spectrometry-based shotgun proteomics. *Nat. Protoc.*, **11**, 2301–2319.
47. Tyanova,S., Temu,T., Sinitcyn,P., Carlson,A., Hein,M.Y., Geiger,T., Mann,M. and Cox,J. (2016) The Perseus computational platform for comprehensive analysis of (prote)omics data. *Nat. Methods*, **13**, 731–740.
48. Harpprecht,L., Baldi,S., Schauer,T., Schmidt,A., Bange,T., Robles,M.S., Kremmer,E., Imhof,A. and Becker,P.B. (2019) A Drosophila cell-free system that senses DNA breaks and triggers phosphorylation signalling. *Nucleic Acids Res.*, **47**, 7444–7459.
49. Becker,P.B. and Wu,C. (1992) Cell-free system for assembly of transcriptionally repressed chromatin from Drosophila embryos. *Mol. Cell. Biol.*, **12**, 2241–2249.
50. Ner,S.S. and Travers,A.A. (1994) HMG-D, the Drosophila melanogaster homologue of HMG 1 protein, is associated with early embryonic chromatin in the absence of histone H1. *EMBO J.*, **13**, 1817–1822.
51. Ner,S.S., Blank,T., Pérez-Paralle,M.L., Grigliatti,T.A., Becker,P.B. and Travers,A.A. (2001) HMG-D and histone H1 interplay during chromatin assembly and early embryogenesis. *J. Biol. Chem.*, **276**, 37569–37576.
52. Oldenkamp,R. and Rowland,B.D. (2022) A walk through the SMC cycle: from catching dnas to shaping the genome. *Mol. Cell*, **82**, 1616–1632.
53. Grau-Bové,X., Navarrete,C., Chiva,C., Pribasnig,T., Antó,M., Torruella,G., Galindo,L.J., Lang,B.F., Moreira,D., López-Garcia,P. *et al.* (2022) A phylogenetic and proteomic reconstruction of eukaryotic chromatin evolution. *Nat. Ecol. Evol.*, **6**, 1007–1023.
54. Chesnokov,I.N. (2007) Multiple functions of the origin recognition complex. *Int. Rev. Cytol.*, **256**, 69–109.
55. Rogers,S.L. and Rogers,G.C. (2008) Culture of Drosophila S2 cells and their use for rnai-mediated loss-of-function studies and immunofluorescence microscopy. *Nat. Protoc.*, **3**, 606–611.